nature synthesis

Review Article

https://doi.org/10.1038/s44160-022-00232-z

Synthesis of atomically thin sheets by the intercalation-based exfoliation of layered materials

In the format provided by the authors and unedited

Supplementary information

for

Synthesis of atomically thin sheets by the intercalation-based exfoliation of layered materials

Ruijie Yang[1,2], Yingying Fan[1,2], Liang Mei[1], Hyeon Suk Shin[3], Damien Voiry[4], Qingye Lu[2], Ju Li[5†], Zhiyuan Zeng[1,6†]

[1]Department of Materials Science and Engineering and State Key Laboratory of Marine Pollution, City University of Hong Kong, 83 Tat Chee Avenue, Kowloon, Hong Kong 999077, P. R. China.

[2]Department of Chemical and Petroleum Engineering, University of Calgary, 2500 University Drive, NW, Calgary, Alberta, T2N 1N4, Canada.

[3]Department of Chemistry, Ulsan National Institute of Science and Technology (UNIST), Ulsan 612022, South Korea.

[4]Institut Européen des Membranes, IEM, UMR 5635, Université Montpellier, ENSCM, CNRS, Montpellier.

[5]Department of Nuclear Science and Engineering and Department of Materials Science and Engineering, Massachusetts Institute of Technology, Cambridge, MA, 02139, USA.

[6]Shenzhen Research Institute, City University of Hong Kong, Shenzhen 518057, China.

[†]E-mail: zhiyzeng@cityu.edu.hk, liju@mit.edu

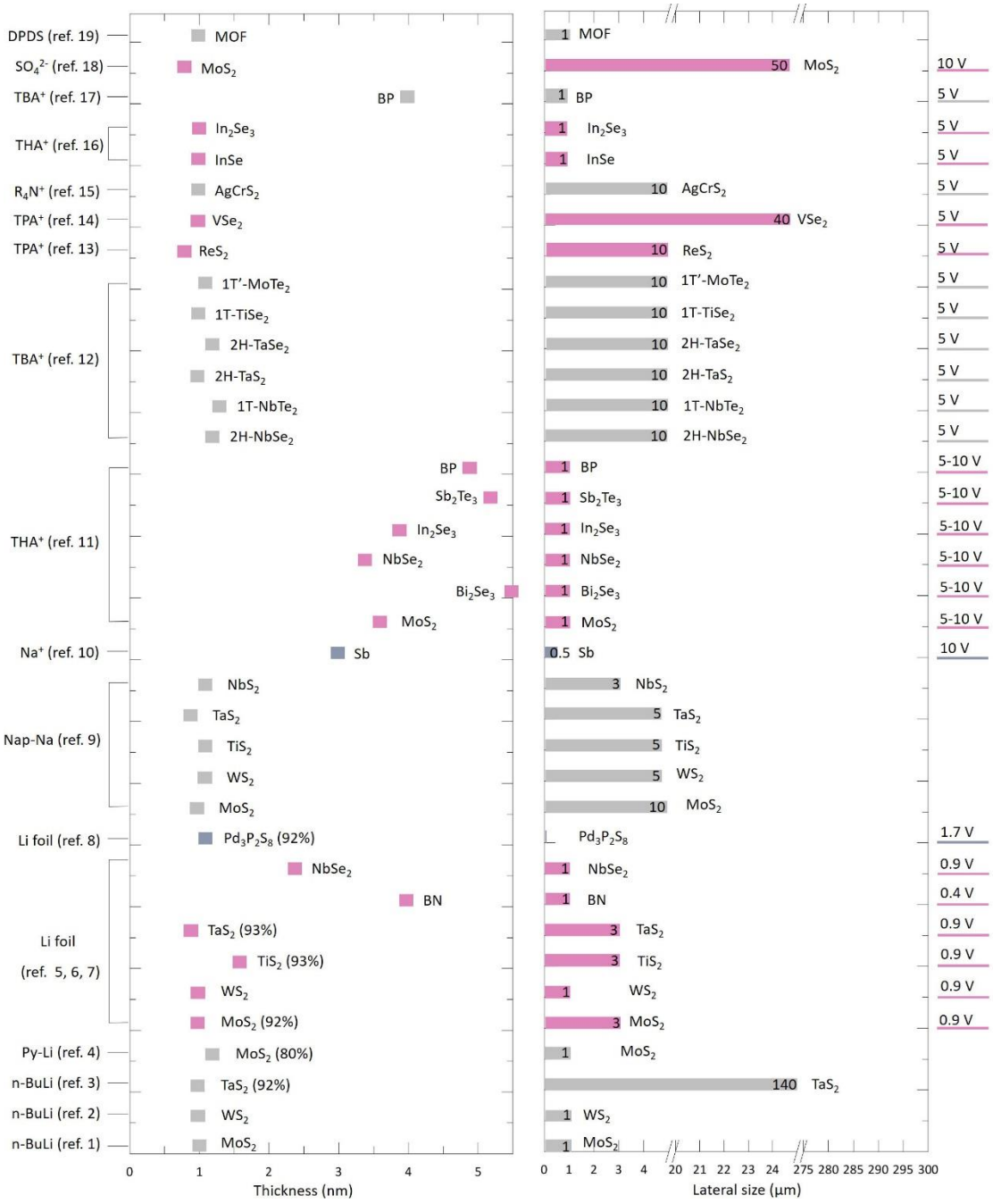

Supplementary Figure 1 | **Summary of product quality (thickness, yield, and lateral size) of various types of intercalation-based exfoliation methods.** Data collected from ref.[1-19]. If the nanosheets are prepared by an electrochemical intercalation-based exfoliation method, the corresponding applied voltage values are listed on the right side of the figure. Of note, the quality of the final products (thickness, yield, lateral size, and others) prepared by intercalation-based exfoliation method is not only related to the intercalant used, but also may be affected by some other experimental conditions, including the applied voltage or current, exfoliation power (*e.g.*, ultrasonic power), etc.

(as shown in **Fig. 5e, f**). Crucially, the quality of the final product (of particular thickness and lateral size) can also be on-demand selected via adjusting the centrifugal speed (As shown in **Fig. 5g**). DPDS: 4,4′-Dipyridyl disulfide; SO_4^{2-}: Sulfate ion; TBA^+: Tetrabutylammonium ion; THA^+: Tetraheptylammonium ion; R_4N^+: Tetraalkylammonium ion; TPA^+: Tetrapropylammonium ion; Na^+: Sodium ion; Nap-Na: Naphthalenide Sodium; Li foil: Lithium foil; Py-Li: pyrene lithium; *n*-BuLi: *n*-Butyllithium.

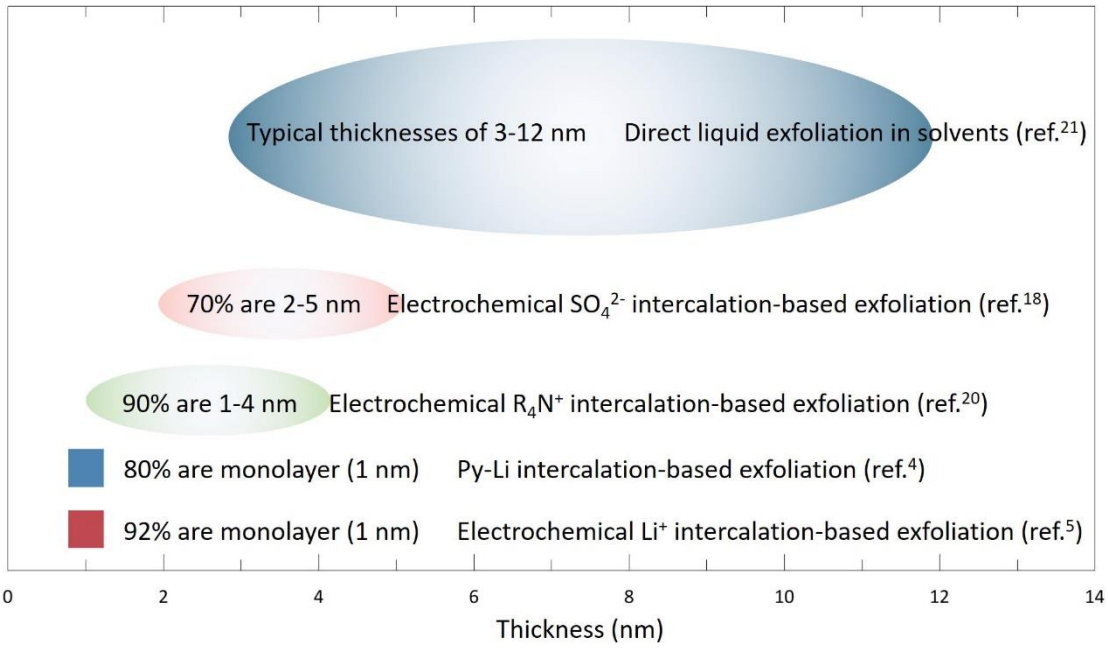

Supplementary Figure 2 | **Comparison of product (take MoS_2 as an example) thickness of intercalation-based exfoliation method and direct liquid exfoliation method.** Data collected from ref.[4,5,18,20,21].

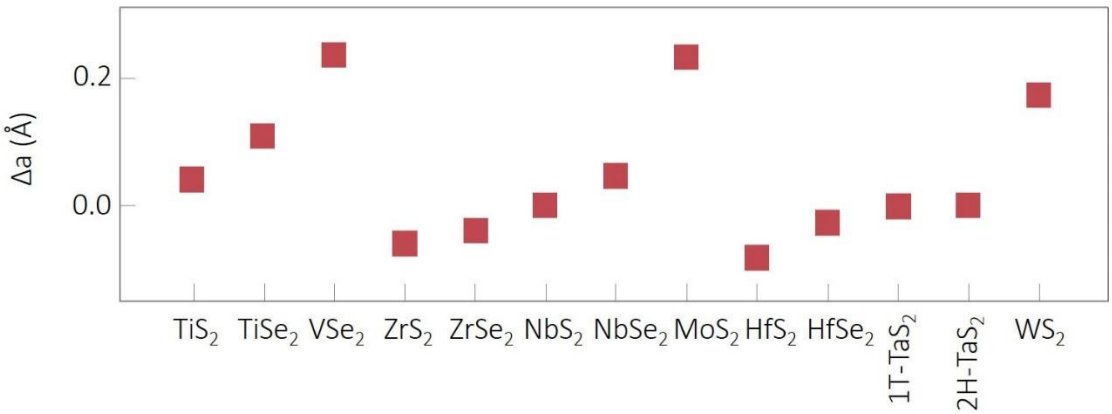

Supplementary Figure 3 | **D-value (difference value) of lattice parameter *a* (Δ*a*) of 13 kinds of TMD materials.** Adapted with permission from ref.[3], American Chemical Society.

Supplementary Table 1 | **A list of tetraalkylammonium cations (R_4N^+) used for the electrochemical intercalation-based exfoliation strategy.**

Abbreviation	Full name	Structural formula
TMA^+	Tetramethylammonium ion	
TEA^+	Tetraethylammonium ion	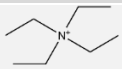
TPA^+	Tetrapropylammonium ion	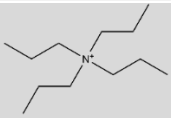
TBA^+	Tetrabutylammonium ion	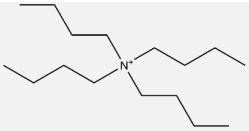
THA^+	Tetraheptylammonium ion	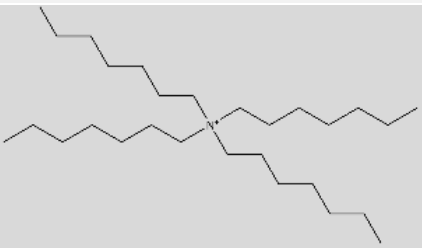
TOA^+	Tetraoctylammonium ion	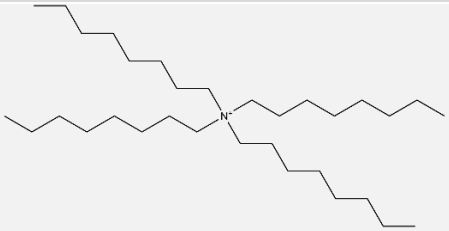

Supplementary Table 2 | **Examples of device applications of exfoliated nanosheets.**

Nanosheet	Intercalation-based exfoliation (IE) method	Deposition technique	Substrate	Device	Performance	Ref.
Graphene	Electrochemical SO_4^{2-} IE	Dip-coating	Si/SiO_2	FET	Field-effect mobility of 17 $cm^2 \cdot V^{-1} \cdot s^{-1}$	22
	Electrochemical SO_4^{2-} IE	Vacuum filtration and dry transfer	PTFE membrane transfer to Si/SiO_2	FET	High hole mobility of ~233 $cm^2 \cdot V^{-1} \cdot s^{-1}$	23
	Electrochemical SO_4^{2-} IE	Brush painting	Commercial A4-size paper	Supercapacitor	High area capacitance of 11.3 $mF \cdot cm^{-2}$, excellent rate capability of 5000 $mV \cdot s^{-1}$.	24
	Electrochemical BF_4^- IE	Vacuum filtration and dry transfer	PTFE membrane transfer to PET	Supercapacitor	High energy density of 56 $mWh \cdot cm^{-3}$	25
MoS_2	Electrochemical SO_4^{2-} IE	Dip-coating	Si/SiO_2	FET	On/off current ratio of 10^6, field-effect mobility of 1.2 $cm^2 \cdot V^{-1} \cdot s^{-1}$	18
	Chemical Li^+ IE	Vacuum filtration	Nylon supports with 200 nm pore size	Nanolaminate membrane	>90% and ~87% rejection rates for micropollutants and NaCl, respectively	26
	Chemical Li^+ IE	Vacuum filtration	Porous PES with 30 nm pore size	Nanolaminate membrane	>90% rejection rates for micropollutants	27

	Chemical Li^+ IE	Vacuum filtration	Celluloseester with 25 nm pore size	Nanolaminate membrane	~92% rejection rates for Na_2SO_4	28
	Electrochemical Li^+ IE	Vacuum filtration	Nylon supports with 220 nm pore size	Nanolaminate membrane	>90% and >80% rejection rates for various dyes and NaCl, respectively	29
	Electrochemical Li^+ IE	Vacuum filtration and transfer	Cellulose acetate filter membrane transfer to polyimide	Supercapacitor	High areal capacitance of 0.63 $F{\cdot}cm^{-2}$, volumetric capacitance of 437 $F{\cdot}cm^{-3}$	30
	Chemical Li^+ IE	Vacuum filtration and transfer	Nitrocellulose membranes transfer to polyimide	Supercapacitor	Capacitance values ranging from ~400 to ~700 $F{\cdot}cm^{-3}$ in a variety of aqueous electrolytes	31
	Chemical Li^+ IE	-	-	Lithium ion battery	Initial charge and discharge capacities are as much as 1113.3/2084.4 $mAh{\cdot}g^{-1}$	4
	Chemical Li^+ IE	-	Si/SiO_2	Photodetector	The responsivity and detectivity of the MoS_2 based photodetector are 0.881 mA/W and 1.28 × 109 Jones at 980 nm and 0.539 mA/W and 0.94 × 109 Jones at 1550 nm, respectively.	32
	Electrochemical THA^+ IE	Spin-coating	Si/SiO_2	TFT	Room-temperature mobilities of about 10 square centimetres per volt per second and on/off ratios of 10^6	11

TaS_2	Chemical Li^+ IE	Vacuum filtration and transfer	Cellulose acetate membrane transfer to glass	Supercapacitor	Large volumetric capacitance of 508 $F \cdot cm^{-3}$ at scan rate of 10 $mV \cdot s^{-1}$ and high energy density of 58.5 $Wh \cdot L^{-1}$	[33]
WS_2	Chemical Li^+ IE	Vacuum filtration	AAO membrane with a pore size of 200 nm	Nanolaminate membrane	93% rejection for EB and 98% for cyt *c*.	[34]
	Chemical Li^+ IE	Vacuum filtration	Filter membrane	Photodetector	Broadband wavelength from visible light to near-infrared light (532–1064 nm), the responsivity is 4.04 mA/W, and the detectivity is 2.55 × 109 Jones at 532 nm irradiation.	[35]
$MoTe_2$	Electrochemical THA^+ IE	Spin-coating	Si/SiO_2	Fiber ring laser cavity	Repetition rate of 3.15 MHz and pulse duration as short as 867 fs at 1563 nm	[36]
BP	Electrochemical TBA^+ IE	Dip-coating	Si/SiO_2	FET	High hole mobility of 76 $cm^2 \cdot V^{-1} \cdot s^{-1}$ and an on/off ratio of 10^3 at 298 K	[37]
	Electrochemical TBA^+ IE	Spin-coating	Si/SiO_2	FET	High hole mobility of 252 ± 18 $cm^2 \cdot V^{-1} \cdot s^{-1}$ and a remarkable on/off ratio of (1.2 ± 0.15) × 10^5 at 143 K	[17]
	Electrochemical TBA^+ IE	Drop-coating	Si/SiO_2	FET	High mean hole mobility of ~60 $cm^2 \cdot V^{-1} \cdot s^{-1}$ (up to ~100 $cm^2 \cdot V^{-1} \cdot s^{-1}$) with a high on/off ratio (~1 × 10^4 in average)	[38]
In_2Se_3	Electrochemical THA^+ IE	Vacuum filtration and dry transfer	PTFE membrane transfer to Si/SiO_2	Photodetector	Ultrafast response time with a rise and decay of 41 and 39 ms, respectively, and efficient responsivity of 1 $mA \cdot W^{-1}$	[39]

	Electrochemical THA^+ IE	Spin-coating	Si/SiO_2	FET	An on/off ratio of more than 10^5 and electron mobility of 0.2 $cm^2 \cdot V^{-1} \cdot s^{-1}$	16
InSe	Electrochemical TBA^+ IE	Drop-casting	FTO	Photodetector	The photoresponse and response time are 10.14 mA/W and 2/37 ms, respectively.	40
Bi_2Se_3	Chemical Li^+ IE	-	ITO	Photodetector	The response time and responsivity are about 0.7 s, and 20.48 mA/W, respectively.	41

IE: Intercalation-based exfoliation

FET: Field effect transistor

PTFE: Polytetrafluoroethylene

PET: Polyethylene terephthalate

PES: Poly(ether sulfone)

TFT: Thin-film transistor

AAO: Anodic alumina oxide

EB: Evans Blue

cyt *c*: cytochrome *c*

FTO: SnO_2:F

ITO: Indium–tin oxide

Supplementary Table 3 | **Examples of catalysis applications of exfoliated nanosheets.**

Nanosheet	Intercalation-based exfoliation (IE) method	Application	Performance	Ref.
MoS_2	Chemical Li^+ IE	Electrocatalytic HER	Electrocatalytic current density of 10 $mA \cdot cm^{-2}$ at a low overpotential of −187 mV vs RHE and a Tafel slope of 43 mV/decade	42
WS_2	Chemical Li^+ IE	Electrocatalytic HER	The TOF reaches 175 s^{-1} at a potential of -288 mV	2
$Pd_3P_2S_8$	Electrochemical Li^+ IE	Electrocatalytic HER	Onset potential of -52 mV, a Tafel slope of 29 mV dec^{-1}	8
Sb	Electrochemical Na^+ IE	Electrocatalytic CO_2RR	FE for formate of 88.5 % at a potential of -0.96 V	10
$ZnIn_2S_4$	Chemical Li^+ IE	Photocatalytic HER	2.258 $mmol \cdot g^{-1} \cdot h^{-1}$	43
BiOCl	Electrochemical Li^+ IE	Photocatalytic CO_2RR	0.1882 $mmol \cdot g^{-1} \cdot h^{-1}$	44

IE: Intercalation-based exfoliation

HER: Hydrogen evolution reaction

CO_2RR: CO_2 reduction reaction

TOF: Turnover frequency

FE: Faraday efficiency

Supplementary Table 4 | **Price list of layered materials. Data and pictures collected from hq-graphene (http://www.hqgraphene.com/index.php).**

Layered materials	Lateral size	Photograph	Price (euro)
MoS_2 (2H Molybdenum Disulfide)	0.8-1 cm		635
$MoSe_2$ (2H Molybdenum Diselenide)	0.8-1 cm		635
$MoTe_2$ (2H Molybdenum Ditelluride)	0.6-0.8 cm	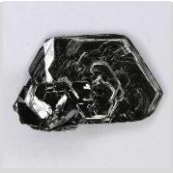	635
WS_2 (2H Tungsten Disulfide)	0.8-1 cm		635
WSe_2 (Tungsten Diselenide)	0.8-1 cm		635
WTe_2 (Tungsten Ditelluride)	0.6-0.8 cm		635
TiS_2 (1T Titanium Disulfide)	0.6-0.8 cm	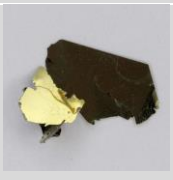	635
$TiSe_2$ (1T Titanium Diselenide)	0.8 cm		635

$TiTe_2$ (Titanium Ditelluride)	0.8 cm		635
$ZrSe_3$ (Zirconium Triselenide)	0.6-0.8 cm		635
$ZrSe_2$ (Zirconium Diselenide)	0.8-1 cm		635
$ZrTe_3$ (Zirconium Tritelluride)	0.6-0.8 cm		635
TaS_2 (2H Tantalum Disulfide)	0.6-0.8 cm		635
$TaSe_2$ (2H Tantalum Diselenide)	0.6-0.8 cm		635
$TaTe_2$ (Tantalum Ditelluride)	0.6-0.8 cm		635
NbS_2 (3R Niobium Disulfide)	0.4 cm		635
$NbSe_2$ (2H Niobium Diselenide)	0.6-0.8 cm		635
$NbTe_2$ (Niobium Ditelluride)	0.6-0.8 cm		635

HfS_2 (Hafnium Disulfide)	0.6-0.8 cm		635
$HfSe_2$ (Hafnium Diselenide)	0.6-0.8 cm		635
$HfTe_2$ (1T Hafnium Ditelluride)	0.6-0.8 cm	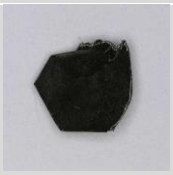	635
VSe_2 (1T Vanadium Diselenide)	0.6-0.8 cm		635
ReS_2 (Rhenium Disulfide)	0.8 cm		635
$ReSe_2$ (Rhenium Diselenide)	0.6-0.8 cm	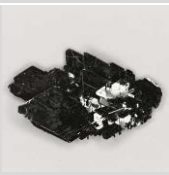	635
$PtSe_2$ (Platina Diselenide)	0.2-0.3 cm		635
$PtTe_2$ (Platina Ditelluride)	0.2-0.3 cm		635
SnS_2 (2H Tin Disulfide)	0.6-0.8 cm		635
$SnSe_2$ (Tin Diselenide)	0.8 cm		635

$PdTe_2$ (Palladium Ditelluride)	0.2-0.3 cm		635
Bi_2S_3 (Bismuth Sulfide)	0.6-0.8 cm		635
Bi_2Se_3 (Bismuth Selenide)	0.6-0.8 cm		635
Bi_2Te_3 (Bismuth Telluride)	0.6-0.8 cm		635
Natural graphite	0.1 cm		180
h-BN (Hexagonal Boron Nitride)	100 μm		635
BP (Black Phosphorus)	0.6-0.8 cm		690

Supplementary Table 5 | **A list of solvents used for the dispersion of $NbSe_2$**[12].

Abbreviation	Full name	Structural formula	Polarity Index
TOL	Toluene	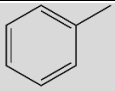	2.4
DCM	Dichloromethane	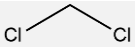	3.1
IPA	Isopropyl Alcohol		4.0
THF	Tetrahydrofuran		4.0
ETAC	Ethyl Acetate	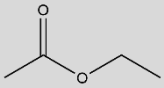	4.4
DIOX	1,4-Dioxane		4.8
ACE	Acetone		5.1
ACN	Acetonitrile	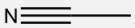	5.8
FA	Formic Acid	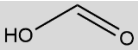	6.0
AA	Acetic Acid	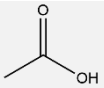	6.0
DMF	N,N-Dimethyl Formamide	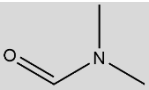	6.4
DMSO	Dimethyl Sulfoxide		7.2

References

1 Eda, G. *et al.* Photoluminescence from Chemically Exfoliated MoS_2. *Nano Lett.* **11**, 5111-5116 (2011).

2 Voiry, D. *et al.* Enhanced catalytic activity in strained chemically exfoliated WS_2 nanosheets for hydrogen evolution. *Nat. Mater.* **12**, 850-855 (2013).

3 Peng, J. *et al.* Very Large-Sized Transition Metal Dichalcogenides Monolayers from Fast Exfoliation by Manual Shaking. *J. Am. Chem. Soc.* **139**, 9019-9025 (2017).

4 Zhu, X. *et al.* Exfoliation of MoS_2 Nanosheets Enabled by a Redox-Potential-Matched Chemical Lithiation Reaction. *Nano Lett.* **22**, 2956-2963 (2022).

5 Zeng, Z. *et al.* Single-Layer Semiconducting Nanosheets: High-Yield Preparation and Device Fabrication. *Angew. Chem. Int. Edit.* **50**, 11093-11097 (2011).

6 Zeng, Z. *et al.* An Effective Method for the Fabrication of Few-Layer-Thick Inorganic Nanosheets. *Angew. Chem. Int. Edit.* **51**, 9052-9056 (2012).

7 Yang, R. *et al.* High-yield production of mono- or few-layer transition metal dichalcogenide nanosheets by an electrochemical lithium ion intercalation-based exfoliation method. *Nat. Protoc.* **17**, 358-377 (2022).

8 Zhang, X. *et al.* Lithiation-induced amorphization of $Pd_3P_2S_8$ for highly efficient hydrogen evolution. *Nat. Catal.* **1**, 460-468 (2018).

9 Zheng, J. *et al.* High yield exfoliation of two-dimensional chalcogenides using sodium naphthalenide. *Nat. Commun.* **5**, 2995 (2014).

10 Li, F. *et al.* Unlocking the Electrocatalytic Activity of Antimony for CO_2 Reduction by Two-Dimensional Engineering of the Bulk Material. *Angew. Chem. Int. Edit.* **56**, 14718-14722 (2017).

11 Lin, Z. *et al.* Solution-processable 2D semiconductors for high-performance large-area electronics. *Nature* **562**, 254-258 (2018).

12 Li, J. *et al.* Printable two-dimensional superconducting monolayers. *Nat. Mater.* **20**, 181-187 (2021).

13 Yu, W. *et al.* Domain Engineering in ReS_2 by Coupling Strain during Electrochemical Exfoliation. *Adv. Funct. Mater.* **30**, 2003057 (2020).

14 Yu, W. *et al.* Chemically Exfoliated VSe_2 Monolayers with Room-Temperature Ferromagnetism. *Adv. Mater.* **31**, 1903779 (2019).

15 Peng, J. *et al.* Stoichiometric two-dimensional non-van der Waals $AgCrS_2$ with superionic behaviour at room temperature. *Nat. Chem.* **13**, 1235-1240 (2021).

16 Lin, Z. *et al.* High-yield exfoliation of 2D semiconductor monolayers and reassembly of organic/inorganic artificial superlattices. *Chem* **7**, 1887-1902 (2021).

17 Yang, S. *et al.* A Delamination Strategy for Thinly Layered Defect-Free High-Mobility Black Phosphorus Flakes. *Angew. Chem. Int. Edit.* **57**, 4677-4681 (2018).

18 Liu, N. *et al.* Large-Area Atomically Thin MoS_2 Nanosheets Prepared Using Electrochemical Exfoliation. *ACS Nano* **8**, 6902-6910 (2014).

19 Ding, Y. *et al.* Controlled Intercalation and Chemical Exfoliation of Layered Metal–Organic Frameworks Using a Chemically Labile Intercalating Agent. *J. Am. Chem. Soc.* **139**, 9136-9139 (2017).

20 Tang, B. *et al.* Wafer-scale solution-processed 2D material analog resistive memory array for memory-based computing. *Nat. Commun.* **13**, 3037 (2022).

21 Coleman, J. N. *et al.* Two-Dimensional Nanosheets Produced by Liquid Exfoliation of Layered Materials. *Science* **331**, 568-571 (2011).

22 Su, C.-Y. *et al.* High-Quality Thin Graphene Films from Fast Electrochemical Exfoliation. *ACS Nano* **5**, 2332-2339 (2011).

23 Parvez, K. *et al.* Electrochemically Exfoliated Graphene as Solution-Processable, Highly Conductive Electrodes for Organic Electronics. *ACS Nano* **7** (2013).

24 Parvez, K. *et al.* Exfoliation of Graphite into Graphene in Aqueous Solutions of Inorganic Salts. *J. Am. Chem. Soc.* **136**, 6083-6091 (2014).

25 Zhou, F. *et al.* Electrochemically Scalable Production of Fluorine-Modified Graphene for Flexible and High-Energy Ionogel-Based Microsupercapacitors.

J. Am. Chem. Soc. **140**, 8198-8205 (2018).

26 Ries, L. *et al.* Enhanced sieving from exfoliated MoS_2 membranes via covalent functionalization. *Nat. Mater.* **18**, 1112-1117 (2019).

27 Wang, Z. *et al.* Understanding the Aqueous Stability and Filtration Capability of MoS_2 Membranes. *Nano Lett.* **17**, 7289-7298 (2017).

28 Hoenig, E. *et al.* Controlling the Structure of MoS_2 Membranes via Covalent Functionalization with Molecular Spacers. *Nano Lett.* **20**, 7844-7851 (2020).

29 Mei, L. *et al.* Simultaneous Electrochemical Exfoliation and Covalent Functionalization of MoS_2 Membrane for Ion Sieving. *Adva. Mater.* **34**, 2201416 (2022).

30 Chen, W. *et al.* Two-dimensional quantum-sheet films with sub-1.2 nm channels for ultrahigh-rate electrochemical capacitance. *Nat. Nanotechnol.* **17**, 153-158 (2022).

31 Acerce, M., Voiry, D. & Chhowalla, M. Metallic 1T phase MoS_2 nanosheets as supercapacitor electrode materials. *Nat. Nanotechnol.* **10**, 313-318 (2015).

32 Park, M. J., Park, K. & Ko, H. Near-infrared photodetector achieved by chemically-exfoliated multilayered MoS2 flakes. *Appl. Surf. Sci.* **448**, 64-70 (2018).

33 Wu, J. *et al.* Acid-Assisted Exfoliation toward Metallic Sub-nanopore TaS_2 Monolayer with High Volumetric Capacitance. *J. Am. Chem. Soc.* **140**, 493-498 (2018).

34 Sun, L. *et al.* Ultrafast Molecule Separation through Layered WS_2 Nanosheet Membranes. *ACS Nano* **8**, 6304-6311 (2014).

35 Li, J., Han, J., Li, H., Fan, X. & Huang, K. Large-area, flexible broadband photodetector based on WS_2 nanosheets films. *Mat. Sci. Semicon. Proc.* **107**, 104804 (2020).

36 Yu, W. *et al.* High-Yield Exfoliation of Monolayer 1T'-$MoTe_2$ as Saturable Absorber for Ultrafast Photonics. *ACS Nano* **15**, 18448-18457 (2021).

37 Wang, N. *et al.* Electrochemical Delamination of Ultralarge Few-Layer Black Phosphorus with a Hydrogen-Free Intercalation Mechanism. *Adv. Mater.* **33**,

2005815 (2021).

38 Li, J. *et al.* Ultrafast Electrochemical Expansion of Black Phosphorus toward High-Yield Synthesis of Few-Layer Phosphorene. *Chem. Mater.* **30**, 2742-2749 (2018).

39 Shi, H. *et al.* Ultrafast Electrochemical Synthesis of Defect-Free In_2Se_3 Flakes for Large-Area Optoelectronics. *Adv. Mater.* **32**, 1907244 (2020).

40 Yang, X. *et al.* Boosting Photoresponse of Self-Powered InSe-Based Photoelectrochemical Photodetectors via Suppression of Interface Doping. *ACS Nano* **16**, 8440-8448 (2022).

41 Zang, C. *et al.* Photoresponse properties of ultrathin Bi_2Se_3 nanosheets synthesized by hydrothermal intercalation and exfoliation route. *Appl. Surf. Sci.* **316**, 341-347 (2014).

42 Lukowski, M. A. *et al.* Enhanced Hydrogen Evolution Catalysis from Chemically Exfoliated Metallic MoS_2 Nanosheets. *J. Am. Chem. Soc.* **135** (2013).

43 Zhang, S. *et al.* MoS_2 Quantum Dot Growth Induced by S Vacancies in a $ZnIn_2S_4$ Monolayer: Atomic-Level Heterostructure for Photocatalytic Hydrogen Production. *ACS Nano* **12**, 751-758 (2018).

44 Shi, Y. *et al.* Van Der Waals gap-rich BiOCl atomic layers realizing efficient, pure-water CO_2-to-CO photocatalysis. *Nat. Commun.* **12**, 5923 (2021).